PHILOSOPHICAL TRANSACTIONS OF THE ROYAL SOCIETY A MATHEMATICAL, PHYSICAL & ENGINEERING SCIENCES

Fractal structures in nonlinear plasma physics

R. L. Viana, E. C. Da Silva, T. Kroetz, I. L. Caldas, M. Roberto and M. A. F. Sanjuán

Phil. Trans. R. Soc. A 2011 **369**, 371-395
doi: 10.1098/rsta.2010.0253

PHILOSOPHICAL TRANSACTIONS OF THE ROYAL SOCIETY A

Phil. Trans. R. Soc. A (2011) **369**, 371–395
doi:10.1098/rsta.2010.0253

Fractal structures in nonlinear plasma physics

By R. L. Viana[1,*], E. C. da Silva[2], T. Kroetz[3], I. L. Caldas[2], M. Roberto[3] and M. A. F. Sanjuán[4,5]

[1]*Departamento de Física, Universidade Federal do Paraná, Caixa Postal 19044, 81531-990, Curitiba, Paraná, Brazil*
[2]*Instituto de Física, Universidade de São Paulo, Caixa Postal 66318, 05315-970, São Paulo, São Paulo, Brazil*
[3]*Instituto Tecnológico de Aeronáutica, Centro Técnico Aeroespacial, Departamento de Física, 12228-900, São José dos Campos, São Paulo, Brazil*
[4]*Nonlinear Dynamics, Chaos and Complex Systems Group, Departamento de Física, Universidad Rey Juan Carlos, Tulipán s/n, 28933 Móstoles, Madrid, Spain*
[5]*Department of Mathematics, School of Science, Beijing Jiaotong University, Beijing 100044, People's Republic of China*

Fractal structures appear in many situations related to the dynamics of conservative as well as dissipative dynamical systems, being a manifestation of chaotic behaviour. In open area-preserving discrete dynamical systems we can find fractal structures in the form of fractal boundaries, associated to escape basins, and even possessing the more general property of Wada. Such systems appear in certain applications in plasma physics, like the magnetic field line behaviour in tokamaks with ergodic limiters. The main purpose of this paper is to show how such fractal structures have observable consequences in terms of the transport properties in the plasma edge of tokamaks, some of which have been experimentally verified. We emphasize the role of the fractal structures in the understanding of mesoscale phenomena in plasmas, such as electromagnetic turbulence.

Keywords: fractal sets; tokamaks; magnetic field lines; area-preserving maps; open Hamiltonian systems

1. Introduction

Fractal geometry, which took its present form in the second half of the twentieth century, has received a great deal of attention after being proved to be necessary to tackle many problems of nonlinear dynamics [1]. An outstanding example is the well-known stretch-and-fold mechanism producing strange attractors, which leads to the fact that most (but not all) chaotic attractors have fractal geometry [2,3]. There are also other fractal chaotic sets of great importance in nonlinear dynamics, such as the so-called strange saddles, which are non-attracting and play a key role in both conservative and dissipative dynamical systems [2]. Moreover, when the dynamical system is multi-stable, i.e. it has more than one coexisting

*Author for correspondence (viana@fisica.ufpr.br).

One contribution of 17 to a Theme Issue 'Nonlinear dynamics in meso and nano scales: fundamental aspects and applications'.

attractor (not necessarily chaotic), it often turns out that the basin boundaries are fractal, leading to difficult issues related to the ability to predict to which attractor a given trajectory will asymptote [4].

The basic building block of fractal structures in nonlinear dynamics is the horseshoe set discovered by Smale [5]: it is constructed from an infinite number of transformations consisting of smoothly stretching and folding onto itself a two-dimensional point set [5]. The set resulting from this infinite sequence of smooth transformations is Cantor-like (self-similar with fractal dimension) and non-attracting. Moreover, the horseshoe set can be shown to contain: (i) a countable set of periodic orbits, (ii) a non-countable set of bounded non-periodic orbits, and (iii) a dense orbit [6].

The ubiquitous presence of fractals in nonlinear dynamics leads to a wealth of fractal structures in nonlinear systems of physical, technological and biological interest [7]. In this paper, we focus on applications in fusion plasmas, specifically the confinement of hot plasmas by externally applied magnetic fields in tokamak devices [8,9]. Tokamak plasmas present many turbulent processes of particle and energy transport, which need to be understood and controlled in order to allow long-lasting plasma confinement for future fusion applications [10,11]. Electromagnetic turbulence in plasmas is a mesoscale phenomenon, characterized by wavelengths intermediate between the ion gyroradius (approx. 1 mm) and the tokamak typical size (approx. 1 m) and time-scales between the Alfvén time (approx. 1–10 ns) and the plasma confinement time (approx. 0.1–10 s) [12].

In this work, we will focus on the magnetic field line structure in tokamaks, which is a lowest order description for the charged particle motion in confined plasmas [8,13,14]. The magnetic field line Lagrangian dynamics gives us valuable hints for the description of the particle behaviour in the presence of electromagnetic turbulence, like its transport properties and anomalous diffusion [10,11,15]. Since the magnetic field is divergence-free, the magnetic field line flow is volume-preserving in phase space, which coincides with the configuration space. Hence, from now on, we identify a trajectory, or orbit, with a field line itself. The configuration may be static, but in this case the role of time is then played by a cyclic (ignorable) spatial coordinate.

Although a symmetric toroidal magnetic confinement configuration is an integrable system (in the Liouville sense), a non-symmetric perturbation turns it into a non-integrable Hamiltonian system where Lagrangian chaos is not only possible but typically found [14,16,17]. This is the case, for example, of the plasma confined in a toroidal scheme (tokamak) with so-called ergodic limiters, which are external electric currents with the purpose of creating a peripheric region of chaotic field lines near the tokamak wall [18–21]. The interest in creating (rather than avoiding) a chaotic region of field lines is the obtaining of a 'cold' boundary layer so as to uniformize heat and particle loadings on the tokamak wall, thus improving the confinement quality through a reduction of impurity releasing [22,23]. Another example of practical application of chaotic field lines in the fusion context is the divertor concept, which needs a chaotic region to drive out undesirable particles from the plasma edge to a collector plate [24–30].

The underlying structure in a chaotic area-preserving orbit is a non-attracting chaotic saddle, and there are many observable manifestations of its fractal character, some of them even having been experimentally verified

[31–34]. An example of a fractal set one can mention is the escape basin, which is the set of initial conditions leading to chaotic orbits which hit the tokamak wall [20,31,35,36]. Besides the escape basin boundaries being fractal sets, they often have the so-called Wada property: every boundary point has an arbitrarily small neighbourhood containing points of all the basins [37–40].

Another example of fractal structure of interest in a toroidal plasma is the magnetic footprints, which is the set of points at which the escaping chaotic orbits reach the tokamak wall [41]. Since charged particles tend to gyrate and drift along magnetic field lines, escaping field lines are preferential transport channels for charged plasma particles [42]. Hence magnetic footprints generate hot spots in barriers like divertor plates with an abnormally high concentration of energy and heat, a feature that has been observed in experiments [31,32].

The main purpose of this paper is to present some fractal structures of interest in the magnetic field line (Lagrangian) dynamics in a tokamak with ergodic limiters. We will show that the chaotic region generated near the tokamak wall does not actually uniformize the loading on the tokamak wall. This non-uniformity is a consequence of the fractal structures associated with the chaotic field line region near the wall, and we show various manifestations of this character, like the connection lengths and magnetic footprints.

This paper is organized as follows. In §2, we make a brief description of the physical system consisting of the symmetric toroidal plasma in a tokamak and the non-symmetric perturbation caused by external electric currents generated by grid-shaped coils called ergodic limiters. In §3, we present the magnetic field line map describing the non-integrable system. Section 4 exhibits some of the fractal structures occurring in the chaotic field line region, namely escape channels and regions of equal connection lengths. Section 5 discusses the relation between the fractal structures and the invariant manifolds of the chaotic saddle corresponding to the chaotic region near the tokamak wall. Section 6 presents escape basins possessing the Wada property and displays examples of magnetic footprints in the tokamak wall. Our conclusions are left to the last section.

2. Model fields

(*a*) *Plasma equilibrium field*

There are many coordinate systems to describe magnetic field lines in a tokamak, its choice depending on the symmetries exhibited by the system [43]. A cylindrical system (R, Z, φ) may be used to describe the tokamak, in which the symmetry (Z-) axis is the major axis of the torus, R is the radial distance from this axis, and φ is the azimuthal angle (figure 1*a*). The torus axis has radius R_0 and a section with $\varphi = \text{const.}$ is a circle of radius b, where a point is located by its polar coordinates (r, θ) [13]. These so-called local coordinates (r, θ, φ), in spite of being simple to define, are not very useful to describe the tokamak equilibrium magnetic field, since a coordinate surface $r = \text{const.}$ does not represent accurately the shape of the confined plasma cross section. To remedy this problem we use a polar toroidal

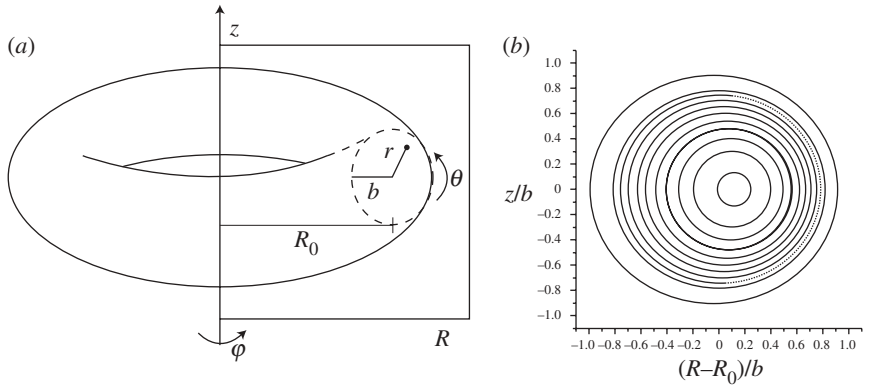

Figure 1. (*a*) Schematic showing the coordinates used to describe magnetic field lines in a tokamak. (*b*) Coordinate curves at a surface intersecting the torus.

coordinate system $(r_t, \theta_t, \varphi_t)$ [44,45] defined by $r_t = \chi(r,\theta)r$, $\sin\theta_t = \chi(r,\theta)\sin\theta$ and $\varphi_t = \varphi$, where

$$\chi^2 = 1 - \frac{r}{R_0'}\cos\theta - \left(\frac{r}{2R_0'}\right)^2 \tag{2.1}$$

and

$$R^2 = R_0'^2\left[1 - \frac{2r_t}{R_0'}\cos\theta_t - \left(\frac{r_t}{R_0'}\right)^2 \sin^2\theta_t\right], \tag{2.2}$$

such that, in the limit $r/R_0' \ll 1$, these coordinates tend to the local ones. The $r_t =$ const. coordinate curves have a pronounced curvature in the interior region of the torus, reflecting an outward displacement of the entire plasma. The intersections of some coordinate surfaces with the plane $\varphi = 0$ are plotted in figure 1*b*. The $r_t = 0$ degenerate surface will be called magnetic axis.

A tokamak plasma in a state of static ideal magnetohydrodynamic (MHD) equilibrium must satisfy the condition $\mathbf{B}_0 \cdot \nabla p_0 = 0$, where $\mathbf{B}_0$ and p_0 are the equilibrium magnetic field and plasma kinetic pressure, respectively. It turns out that the equilibrium magnetic field lines lie on constant pressure surfaces with topology of nested tori, known as *magnetic surfaces* [9,46]. The existence of magnetic surfaces is a necessary (but not sufficient) condition for plasma confinement. In addition, to present closed magnetic surfaces the system must have some spatial symmetry. In tokamaks, we assume symmetry with respect to the azimuthal angle φ [9]. Accordingly, we have chosen a system for which the coordinate surfaces coincide with magnetic surfaces.

Instead of the pressure, we may label magnetic surfaces with other surface quantities, like the poloidal magnetic flux $\Psi_p(r_t, \theta_t)$, defined as the flux of $\mathbf{B}_0$ through a ribbon from the magnetic axis to a coordinate curve, such that the equilibrium condition is $\mathbf{B}_0 \cdot \nabla\Psi_p = 0$. The ideal MHD equations, when applied to

this situation, lead to the so-called Grad–Shafranov–Schlüter equation for the poloidal magnetic flux [9]. It reads, in the polar toroidal system [44,45]

$$\frac{1}{r_t}\frac{\partial}{\partial r_t}\left(r_t\frac{\partial \Psi_p}{\partial r_t}\right)+\frac{1}{r_t^2}\frac{\partial^2 \Psi_p}{\partial \theta_t^2}=\mu_0 J_{30}(\Psi_p)+\mu_0 {R_0'}^2\frac{dp_0}{d\Psi_p}\left(2\frac{r_t}{R_0'}\cos\theta_t+\frac{r_t^2}{{R_0'}^2}\sin^2\theta_t\right)+\frac{r_t}{R_0'}\left[\cos\theta_t\left(2\frac{\partial^2\Psi_p}{\partial r_t^2}+\frac{1}{r_t}\frac{\partial\Psi_p}{\partial r_t}\right)+\sin\theta_t\left(\frac{1}{r_t^2}\frac{\partial\Psi_p}{\partial\theta_t}-\frac{2}{r_t}\frac{\partial^2\Psi_p}{\partial\theta_t\partial r_t}\right)\right], \tag{2.3}$$

where J_{30} is the toroidal component of the equilibrium plasma current density given by

$$J_{30}(\Psi_p)=-R_0'^2\frac{dp_0}{d\Psi_p}-\frac{d}{d\Psi_p}\left(\frac{1}{2}\mu_0 I^2\right), \tag{2.4}$$

where $I=I(r_t,\theta_t)$ is the poloidal current function, which is the current density flux through the same surface used in the definition of Ψ_p. The equilibrium magnetic field contravariant components, in terms of the surface functions Ψ_p and I, are

$${B_0}^1(r_t,\theta_t)=-\frac{1}{R_0' r_t}\frac{\partial\Psi_p}{\partial\theta_t},\quad {B_0}^2(r_t,\theta_t)=\frac{1}{R_0' r_t}\frac{\partial\Psi_p}{\partial r_t},\quad {B_0}^3(r_t,\theta_t)=-\frac{\mu_0 I}{R^2}. \tag{2.5}$$

In order to solve equation (2.3) we have to assume a specific form for the spatial profile of the toroidal current density J_{30}, like

$$J_{30}(r_t)=\frac{I_p R_0'}{\pi a^2}(\gamma+1)\left(1-\frac{r_t^2}{a^2}\right)^{\gamma}, \tag{2.6}$$

where I_p is the total plasma current, a the plasma radius and γ a positive constant. Solving equation (2.3) through a perturbation scheme (where the small parameter is the ratio b/R_0) gives a poloidal flux function, from which the equilibrium field is given by (2.5) [44,45]. Another way to display the equilibrium field is to characterize the magnetic surfaces $\Psi_p=\text{const.}$ by the so-called *safety factor* $q=q(r_t,\theta_t)$, which gives the average poloidal angle swept by the field line after one complete toroidal turn, and which exhibits a monotonic radial profile given by

$$q(r_t\theta_t)=\frac{I_e}{I_p}\frac{r_t^2}{{R_0'}^2}\left[1-\left(1-\frac{r_t^2}{a^2}\right)^{\gamma+1}\right]^{-1}\left(1-4\frac{r_t^2}{{R_0'}^2}\right)^{-1/2}, \tag{2.7}$$

where in lowest order, $I\approx -I_e/2\pi$.

(*b*) *Ergodic limiter field*

As stated in §1, the main goal of the ergodic limiter is to create an outer layer (i.e. near the tokamak wall) of chaotic magnetic field lines [22,23,47]. When this concept appeared, the word 'chaos' was not widely used by plasma physicists, and the word 'ergodic' was used instead. Although the meaning of these words is different, the latter denomination was often maintained for historical reasons.

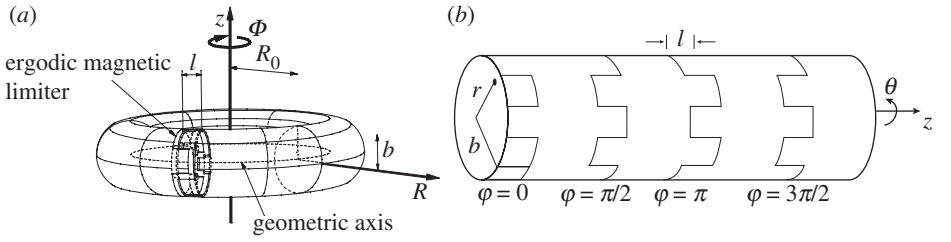

Figure 2. Schematic showing the ergodic limiter in (*a*) toroidal and (*b*) periodic cylindrical configurations.

One of the designs proposed for the ergodic limiter consists of N_a current rings located symmetrically along the toroidal circumference of the tokamak, each of them being a slice of length ℓ of a helical winding characterized by the 'mode numbers' (m_0, n_0), where m_0 and n_0 are co-prime integers, and carrying an electric current I_h (figure 2*a*) [48–50]. In figure 2*b*, we show schematically $N_a = 4$ equally spaced rings along the tokamak in the periodic cylindrical geometry.

The meaning of the mode numbers (m_0, n_0) for a helical winding is that a conductor is wound around the tokamak such that it closes on itself after m_0 turns around the poloidal direction and n_0 turns around the toroidal direction. These mode numbers have to be chosen carefully so as to produce the required chaotic region in the proper region of the plasma (i.e. near the tokamak wall). The procedure involved is based on Hamiltonian theory, since the field line dynamics is a one-degree-of-freedom system with a 'time'-dependent perturbation, which enables us to use powerful theoretical results like KAM theory and so on [13]. A perturbation generated by a helical winding with mode numbers (m_0, n_0) will influence chiefly the resonant magnetic surface for which the safety factor is a rational number m_0/n_0 [19,21,51]. In the cylindrical (lowest order) approximation, if the helical windings were continuous, the only effect would be the appearance of pendular-shaped islands centred at the radius $\bar{r}$ given by $q(\bar{r}) = m_0/n_0$ [19,21,51]. Choosing $\bar{r}$ to be near the plasma radius a we have several possibilities for the mode numbers, like $m_0 = 5$ and $n_0 = 1$, which we will use hereafter. However, since the winding is sliced into discontinuous pieces of small length $\ell \ll 2\pi R_0$, the axisymmetry is broken and chaotic field lines appear near the separatrices of these islands.

Larger regions of chaotic field lines can appear by interaction of the main island related to (m_0, n_0) and its satellite islands created by the toroidal effect. According to the Poincaré–Birkhoff theorem all rational surfaces are destroyed under a non-integrable perturbation [13]. However, even though a non-symmetric perturbation would create periodic islands over all the places of the plasma column, this effect is noticeable only near the plasma edge, where the magnetic field of the limiter is more pronounced. In fact, this magnetic field decays very fast with the distance from the wall, such that the chaotic region produced by the ergodic limiter does not destroy the inner plasma core.

On neglecting the plasma response to the field generated by an ergodic limiter (an acceptable approximation provided the plasma is not at a marginal equilibrium state), the latter may be considered a vacuum field given by $\mathbf{B}_1 = \nabla\Phi_1$, where $\Phi_1(r_t, \theta_t, \varphi)$ is a magnetic scalar potential satisfying the Laplace equation. Ignoring at first the finite extension of the limiter rings, boundary conditions

are fixed in the form of a helical winding the pitch of which emulates the actual field line curvature in the equilibrium configuration, such that the angle $u_t \equiv m_0(\theta_t + \lambda \sin\theta_t) - n_0\varphi$ must be constant along such a helical winding, which is accomplished by conveniently choosing the parameter λ. For a 5/1 helical winding, such as that used in this work, we choose $\lambda = 0.5902$ [21].

The magnetic field $\mathbf{B}_1 = \nabla \times \mathbf{A}_1$ produced by such a configuration is given, in lowest order, by $\mathbf{A}_1 = (0, 0, A_{13})$, where [21]

$$A_{13}(r_t, \theta_t, \varphi) = -\frac{\mu_0 I_h R_0'}{\pi} \sum_{k=-m_0}^{+m_0} J_k(m_0\lambda)\left(\frac{r_t}{b}\right)^{m_0+k} e^{i[(m_0+k)\theta_t - n_0\varphi]}, \tag{2.8}$$

from which the limiter field contravariant components are given by

$$B_1^1(r_t, \theta_t) = -\frac{1}{R_0' r_t}\frac{\partial A_{13}}{\partial \theta_t}, \quad B_1^2(r_t, \theta_t) = \frac{1}{R_0' r_t}\frac{\partial A_{13}}{\partial r_t}, \quad B_1^3 = 0, \tag{2.9}$$

and the model field will be the superposition of the equilibrium and limiter fields: $\mathbf{B} = \mathbf{B}_0 + \mathbf{B}_1$.

3. Magnetic field line map

(*a*) *Hamiltonian form*

Combining the results of the previous section for both equilibrium and limiter fields, there results that the magnetic field line equations are [21]

$$\frac{dr_t}{d\varphi} = -\frac{1}{r_t B_T}\left(1 - 2\frac{r_t}{R_0'}\cos\theta_t\right)\frac{\partial}{\partial \theta_t}\left[\Psi_{p0}(r_t) + A_{13}(r_t, \theta_t, \varphi)\right] \tag{3.1}$$

and

$$\frac{d\theta_t}{d\varphi} = \frac{1}{r_t B_T}\left(1 - 2\frac{r_t}{R_0'}\cos\theta_t\right)\frac{\partial}{\partial r_t}\left[\Psi_{p0}(r_t) + A_{13}(r_t, \theta_t, \varphi)\right], \tag{3.2}$$

where $B_T \equiv \mu_0 I_e / 2\pi R_0'$ is the toroidal magnetic field on the magnetic axis.

It has been long known that this problem can be cast into a Hamiltonian form, by defining a time-like variable as the ignorable coordinate in the equilibrium (axisymmetric) case φ. The canonical angle is chosen as a function of the equilibrium safety factor [52]

$$\vartheta(r_t, \theta_t) = \frac{1}{q(r_t)}\int_0^{\theta_t} \frac{B_0^3(r_t, \theta_t)}{B_0^2(r_t, \theta_t)}\, d\theta = 2\arctan\left[\frac{1}{\Omega(r_t)}\left(\frac{\sin\theta_t}{1+\cos\theta_t}\right)\right], \tag{3.3}$$

where

$$\Omega(r_t) = \left(1 - 2\frac{r_t}{R_0'}\right)^{1/2}\left(1 + 2\frac{r_t}{R_0'}\right)^{-1/2}, \tag{3.4}$$

in such a way that the resonant helical windings are characterized by $m_0\vartheta(r_t, \theta_t) - n_0\varphi_t = \text{constant}$. Expanding equation (3.3) in Fourier series, and retaining only the lowest order non-vanishing correction, there results $\vartheta(\theta_t) = \theta_t + \lambda \sin\theta_t$.

The action canonically conjugated to the angle ϑ is defined in terms of the normalized toroidal magnetic flux

$$\mathcal{J}(r_{\rm t}) = \frac{1}{2\pi R_0'^2 B_{\rm T}} \int \mathbf{B}_0 . \mathbf{d}\boldsymbol{\sigma}_3 = \frac{1}{4}\left[1 - \left(1 - 4\frac{r_{\rm t}^2}{R_0'^2}\right)^{1/2}\right], \tag{3.5}$$

where $\mathbf{d}\boldsymbol{\sigma}_3 = R_0' r_{\rm t}\, {\rm d}r_{\rm t}\, {\rm d}\theta_{\rm t}\hat{e}^3$.

With these formal identifications the field line equations (3.1) can be expressed in a canonical form [43,46]

$$\frac{{\rm d}\mathcal{J}}{{\rm d}\varphi} = -\frac{\partial H}{\partial \vartheta}, \quad \frac{{\rm d}\vartheta}{{\rm d}\varphi} = \frac{\partial H}{\partial \mathcal{J}}, \tag{3.6}$$

where we defined the Hamiltonian

$$H(\mathcal{J},\vartheta,\varphi) = H_0(\mathcal{J}) + H_1(\mathcal{J},\vartheta,\varphi) = \frac{1}{B_{\rm T} R_0'^2}\Psi_{p0}(\mathcal{J}) + \frac{1}{B_{\rm T} R_0'^2} A_{13}(\mathcal{J},\vartheta,\varphi). \tag{3.7}$$

Up to now, we have not taken into account the finite extension of the limiter rings, which is an essential ingredient in the formalism since it is the source of the 'time' dependence of the Hamiltonian, and thus to the integrability breakdown necessary to have chaotic field lines [50]. If the ring length ℓ is small enough, we can model the perturbation associated to the limiters as a sequence of delta-functions centred at each ring position

$$H_{\rm L}(\mathcal{J},\vartheta,\varphi) = H_0(\mathcal{J}) + \frac{\ell}{R_0'} H_1(\mathcal{J},\vartheta,\varphi) \sum_{k=-\infty}^{+\infty} \delta\left(\varphi - k\frac{2\pi}{N_a}\right). \tag{3.8}$$

(*b*) *Map equations*

Discrete-time dynamical systems, also called maps, are important tools for both Hamiltonian and dissipative dynamical systems, since many general results are nicely illustrated by using them, besides being much more easily solved numerically than differential equations [17,46,53,54]. Accordingly, we call $\mathcal{J}_k$ and ϑ_k the action and angle variables, respectively, at the kth crossing of a field line with the plane $\varphi_k = 2\pi k/N_a$ corresponding to each limiter ring along one toroidal turn along the torus, for which $k = 0, 1, 2, \ldots, N_a - 1$. The impulsive character of the perturbation in the Hamiltonian (3.8) enables us to obtain analytically such functions. From the Hamilton equations (3.6) we obtain by integration the following area-preserving mapping for the near-integrable system [21]:

$$\mathcal{J}_{n+1} = \mathcal{J}_n - \epsilon\left(\frac{\partial H_1}{\partial \vartheta}\right)(\mathcal{J}_{n+1}, \vartheta_n, \varphi_n) \tag{3.9}$$

and

$$\vartheta_{n+1} = \vartheta_n + \frac{2\pi}{N_a q(\mathcal{J}_{n+1})} + \epsilon\left(\frac{\partial H_1}{\partial \mathcal{J}}\right)(\mathcal{J}_{n+1}, \vartheta_n, \varphi_n), \tag{3.10}$$

where $\varphi_{n+1} = \varphi_n + (2\pi n/N_a)$, and $\epsilon \equiv -2(\ell/2\pi R_0')(I_h/I)$ is a dimensionless perturbation parameter, and the perturbation owing to the ergodic limiter can be expressed as a Fourier series

$$H_1(\mathcal{J}, \vartheta, \varphi) = \sum_{n=0}^{2m_0} H_n^*(\mathcal{J})\, \mathrm{e}^{\mathrm{i}(n\vartheta - n_0\varphi)}, \tag{3.11}$$

with coefficients given by [21]

$$H_m^*(\mathcal{J}) = \sum_{m'=0}^{2m_0} H_{m'}(r_t(\mathcal{J}))S_{m,m'}(\mathcal{J}), \tag{3.12}$$

in which we defined

$$H_{m'}(r_t) = -J_{m'-m_0}(m_0\lambda)\left(\frac{r_t}{b_t}\right)^{m'} \tag{3.13}$$

and

$$S_{m,m'}(\mathcal{J}) = (-1)^m\left(\frac{c_1(\mathcal{J})}{c_2(\mathcal{J})}\right)^{m+m'} \sum_{n=0}^{m} (-1)^n \alpha_n(m, m')\left(\frac{c_1(\mathcal{J})}{c_2(\mathcal{J})}\right)^{-2n}, \tag{3.14}$$

where J_m is the Bessel function of order m and

$$c_1(\mathcal{J}) = 1 - \frac{1}{\Omega(r_t(\mathcal{J}))}, \quad c_2(\mathcal{J}) = 1 + \frac{1}{\Omega(r_t(\mathcal{J}))}, \tag{3.15}$$

and

$$\alpha_n(m, m') = \begin{cases} 1 & \text{if } m = 0 \quad \text{and} \quad n = 0, \\ m' & \text{if } m = 1 \quad \text{and} \quad n = 0 \quad \text{or} \quad n = 1, \\ m'\dfrac{(m + m' - n - 1)!}{(m - n)!(m' - n)!n!} & \text{if } m > 1 \quad \text{and} \quad n \le m', \\ 0 & \text{if } m > 1 \quad \text{and} \quad n > m'. \end{cases} \tag{3.16}$$

(*c*) *Phase portraits*

In the following numerical results we choose the equilibrium safety factor $q \approx 1$ at the magnetic axis and $q \approx 5$ at the plasma radius ($r_t = a$). We also normalize lengths to the minor radius ($b = 1$) and choose parameters so that $a/R_0' = 0.26$ and $\gamma = 3$, which are values typical for tokamak discharges. We consider $N_a = 4$ limiter rings, each of them with length $\ell = 0.08\,\mathrm{m}$ and mode numbers $m_0 = 5$ and $n_0 = 1$, for the reasons explained in the previous section. The control parameter is the normalized perturbation strength ϵ.

The effect of increasing perturbation on the field line structure, as revealed by the Poincaré surface of section fixed at the $\varphi = 0$ plane, can be appreciated from figure 3, where we rectified the curvature along ϑ for ease of visualization. The tokamak radius, where the limiter rings are mounted, corresponds to the upper boundary of the diagrams, at $\mathcal{J} \approx 0.055$. For a weak perturbation (figure 3*a*, corresponding physically to a limiter current of 1.14% of the plasma current) we

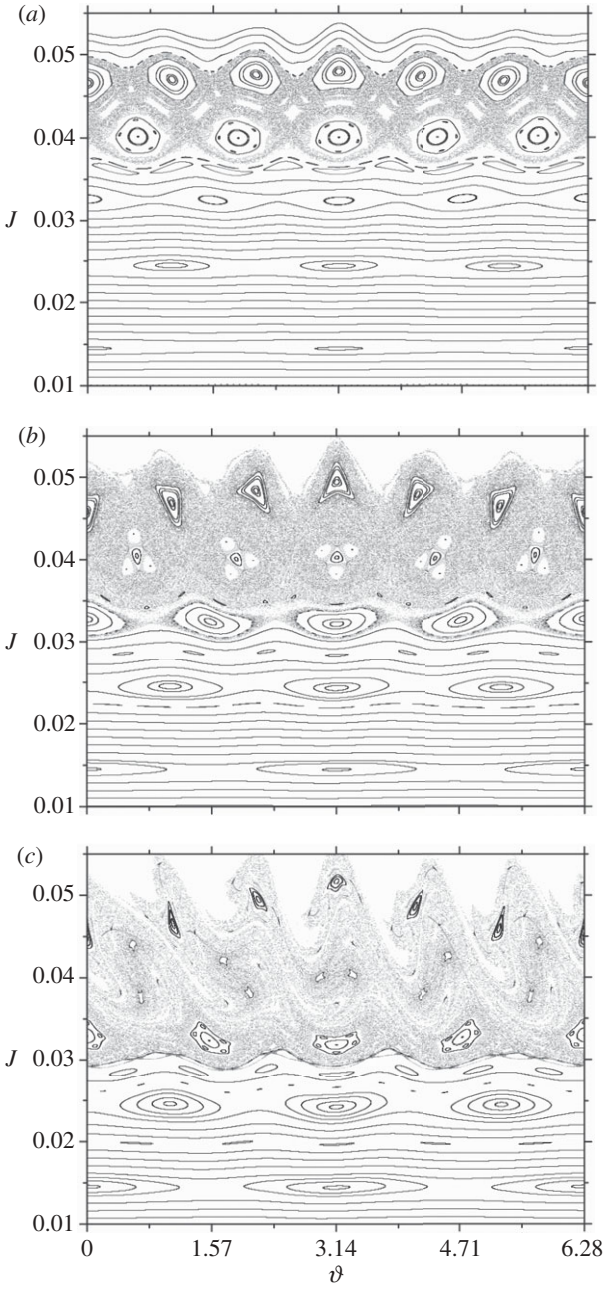

Figure 3. Phase portraits of the field line map (3.9)–(3.10) for increasing perturbation strengths: (*a*) $\epsilon = 1.00 \times 10^{-5}$; (*b*) $\epsilon = 1.20 \times 10^{-4}$; (*c*) $\epsilon = 2.14 \times 10^{-4}$. The upper horizontal line represents the tokamak wall.

observe a pendular chain of five islands centred at $\mathcal{J} \approx 0.04$, which corresponds to the magnetic surface most influenced by the perturbation caused by a $(5, 1)$ mode. Other rational surfaces are likewise perturbed, causing the appearance of

many other chains, like those with three, four and six islands at both sides of the $(5,1)$ chain. Since, from (2.8), the limiter field falls off with decreasing $\mathcal{J}$ the wider islands are those closer to the tokamak wall.

The finite extension of the limiters causes the breakdown of integrability that makes possible the existence of area-filling chaotic field lines (in the Lagrangian sense). As the perturbation increases (figure 3*b*, for a limiter current of 2.73% of the plasma current), neighbour islands interact such that the chaotic layer, previously attached to the islands' separatrices, becomes wider and eventually touches the tokamak wall (figure 3*c*, where I_{H} is 4.86% of I_{P}). The resulting chaotic boundary layer is 'cold' in the sense that particle transport there is faster than within the plasma it encircles [20].

4. Escape channels and connection lengths

The ergodic limiter concept was essentially based on the appealing idea that the chaotic field line region would make uniform the heat and particle loading on the tokamak wall, thus reducing localized attacks which could provoke plasma contamination through sputtering processes and releasing of impurities from the plasma wall [22,23]. This claim is only partially correct though, for the chaotic region *is not uniform*. There are parts of the plasma wall that turn out to be more intensely hit by particles released from the plasma core and a non-uniform (actually fractal) pattern is produced there [31,32].

We consider now the situation depicted in figure 3*b*, for which there is a wide chaotic region that encircles the plasma and touches the tokamak wall. We remark that, for figure 3*a*, the chaotic region does not reach the tokamak wall and so this case is not suitable for operation of an ergodic limiter. For most initial conditions $(\mathcal{J}_0, \vartheta_0)$ picked up within this region, the subsequent iterations of the map generate field lines that eventually hit the tokamak wall. From the physical point of view, these lines are lost and are not reinjected to the tokamak region. Hence we deal with an open Hamiltonian system, like a billiard with holes by which particles can escape through after some time [55–58].

In order to quantify the non-uniformity of the chaotic region depicted in figure 3*b*, we plot in figure 4 the connection lengths, or the 'time' it takes (rather the number of toroidal turns along the tokamak divided by N_a) for a given initial condition $(\mathcal{J}_0, \vartheta_0, \varphi_0 = 0)$ to generate a field line that eventually hits the tokamak wall. The region comprising the tokamak interior was covered with a fine mesh of points, each of them representing an initial condition that is iterated until the corresponding field line is lost, the corresponding connection length being represented in a colour scale.

As we would expect, most of the points immediately near the tokamak wall have small connection lengths (much less than *ca* 100 toroidal turns), but we can find many regions touching the wall with higher connection lengths (of the order of 1000 turns and even higher). There are, however, very large connection lengths that are not related to the chaotic region itself but rather to the interior of the remnant island, which are trajectories bounded by KAM tori and that will never reach the tokamak wall (infinite connection length). The chaotic region near the tokamak wall is clearly non-uniform for there are points with widely different connection lengths, a fact already appreciated in earlier works [32,59,60].

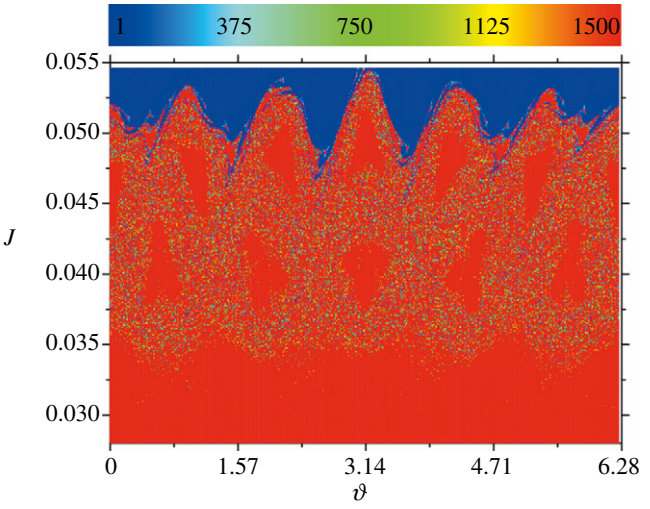

Figure 4. Connection lengths for $\epsilon = 1.2 \times 10^{-4}$. The colour scale indicates the 'time' (measured in number of toroidal turns) it takes for a given field line to hit the tokamak wall. (Online version in colour.)

Another noteworthy feature of the connection length distribution is that not only is it not uniform throughout the chaotic region but regions of different connection lengths are intermixed in fine scales [32,60]. This is illustrated in figure 5, where the connection lengths are plotted for the case of a stronger perturbation, the phase portrait of which is shown in figure 3*c*, where we also present two magnifications of regions inside the highly non-uniform chaotic layer, suggesting that regions of large and small connection lengths are densely mixed. The apparent self-similarity by these magnifications is, in fact, a fractal structure.

The regions of large connection lengths touching the tokamak wall may be thought of as 'low spots' where relatively less particles collide with the vessel, whereas the small connection lengths are 'hot spots', where more particles hit the tokamak wall [28,41,61]. Moreover, there are regions of small connection lengths also in the vicinity of the plasma core (where the connection lengths are infinitely large), forming *escape channels* by which energetic particles from the plasma core are drained rapidly towards the tokamak wall [28,61]. Recent investigations show that the fractal structure of the escape channels affects the overall transport properties in the plasma edge, leading to an abnormal increase of the diffusion coefficient of plasma particles [14,32,49]. This may be one of the reasons why conventional transport (e.g. neoclassical) theories fail to predict the experimentally observed diffusion coefficients of tokamak plasmas [8].

Another feature of the non-uniform character of the chaotic region is shown in figure 6, where we plot (in colour scale) the connection lengths of points immediately close to the tokamak wall (i.e. the strip $(\mathcal{J} = 0.055, 0 \leq \vartheta \leq 2\pi)$) as a function of an equilibrium parameter $q(a)$, which is the safety profile at the plasma radius. For the same perturbation strength, the hot and cold spots on the tokamak wall change their positions according to the equilibrium properties of the magnetic field, for both weak (figure 6*a*) and strong (figure 6*b*) perturbations. Regions with same connection lengths have the shape of 'boomerangs' but the

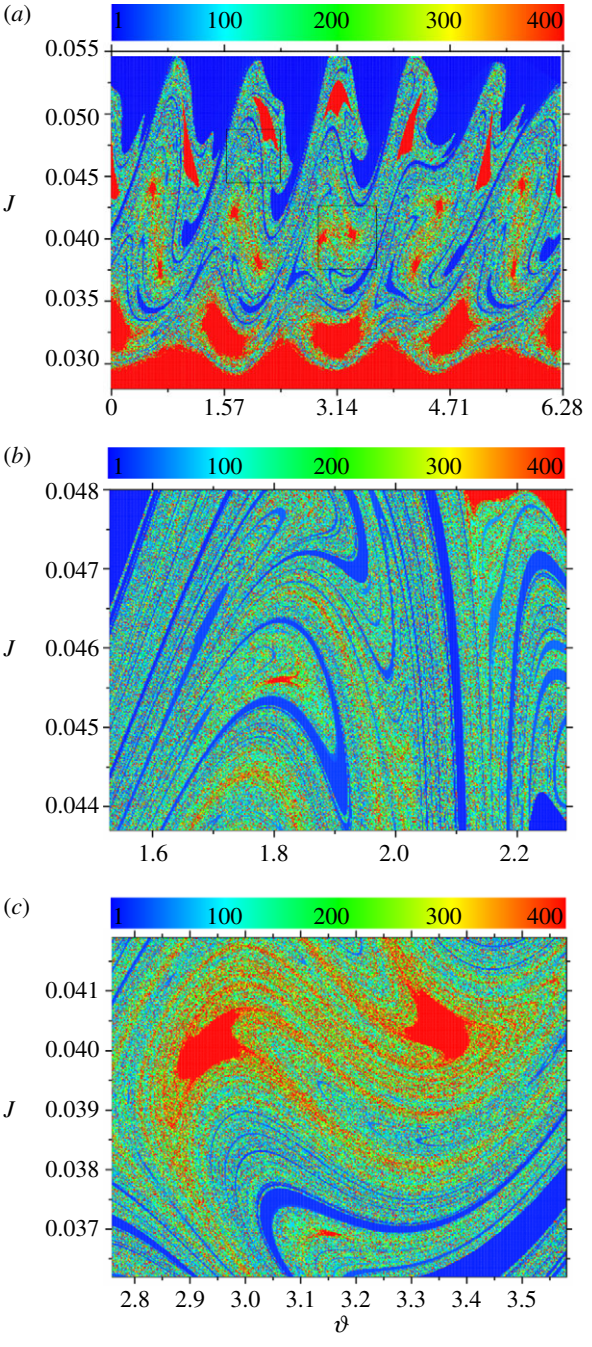

Figure 5. (*a*) Connection lengths for $\epsilon = 2.14 \times 10^{-4}$. The colour scale indicates the 'time' (measured in number of toroidal turns) it takes for a given field line to hit the tokamak wall. (*b*,*c*) Magnifications of selected rectangles in (*a*). (Online version in colour.)

ordering of the colours is not monotonic, inasmuch as there are abrupt jumps among regions of small and large connection lengths that can be regarded as yet another consequence of fractality.

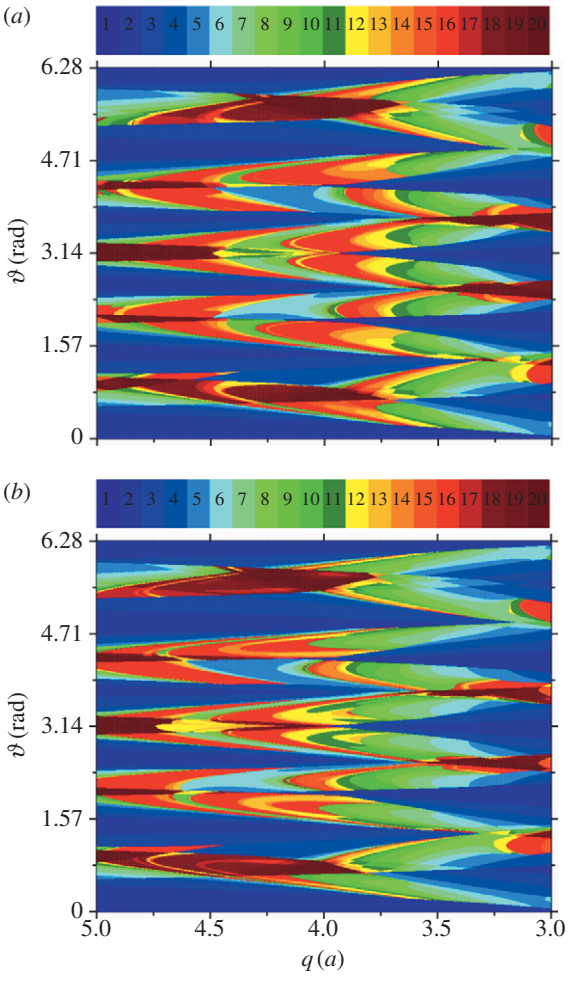

Figure 6. The colour scales indicate the connection lengths just below the tokamak wall as a function of the equilibrium safety factor at plasma edge for (*a*) $\epsilon = 1.2 \times 10^{-4}$ and (*b*) $\epsilon = 2.14 \times 10^{-4}$. (Online version in colour.)

5. Invariant manifolds and chaotic saddle

The results shown in the previous section can be explained by the periodic orbit structure underlying the chaotic orbits of Hamiltonian systems. Let us consider an unstable periodic orbit (period-k saddle) embedded in the chaotic region of any of the phase portraits depicted in figure 3. The stable (unstable) manifold at this point is the set of points which asymptote to the periodic orbit under the forward (backward) iterations of the map (3.9)–(3.10) as 'time' n goes to infinity [13]. The sets are invariant for map iterations of points belonging to these manifolds remain there for all times. A chaotic saddle is a non-attracting chaotic invariant set formed by the intersection of the stable and unstable manifolds of unstable saddle points, and also contains a dense orbit [62]. The stable and unstable manifolds

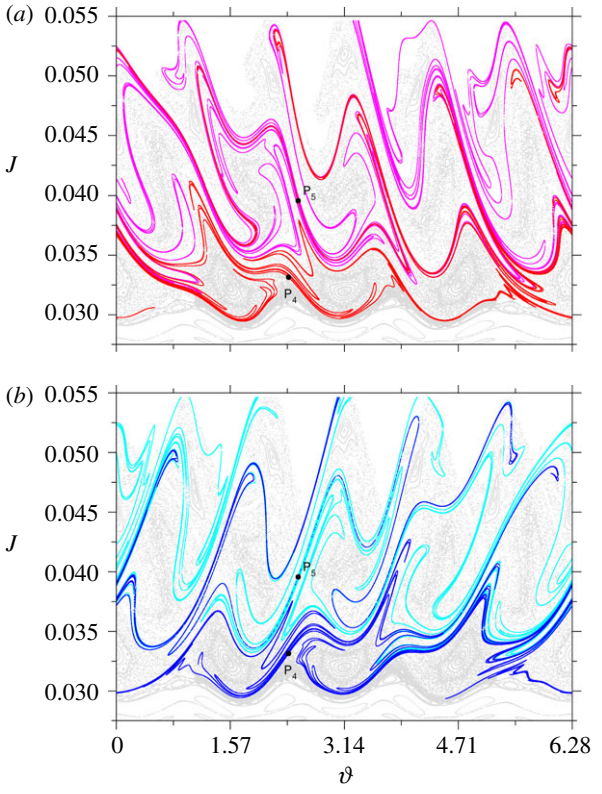

Figure 7. (*a*) Stable and (*b*) unstable manifolds for two unstable fixed points embedded in the chaotic region obtained for $\epsilon = 2.14 \times 10^{-4}$. (Online version in colour.)

intersect transversally at homoclinic or heteroclinic points, and these points map one another, such that there is an infinite number of unstable points embedded in the chaotic saddle [2,3].

Numerical approximations of these manifolds can be obtained from several techniques, like the *sprinkler method* [63], by which we partition the phase portrait in the chaotic region of interest using a fine mesh of points, and iterate each grid point n times. Once the resulting field line trajectory reaches the wall for finite n it is considered lost and the further iterates are not plotted. We pass to the next grid point and so on. For sufficiently large n and a fine enough grid, trajectories that do not hit the wall in n iterates can be used to generate an approximation to the unstable manifold. The unstable manifold structures related to the chaotic regions depicted in figure 3*c* are shown in figure 7*a*. The red and magenta curves correspond to approximations of the unstable manifold branches stemming from unstable fixed points labelled as P_4 and P_5 in figure 7*a*, and belonging originally to the chains with mode numbers (4/1) and (5, 1), respectively.

Although, for time n large enough, both manifolds will reach the tokamak wall, for a fixed n the manifold coloured as magenta will hit the tokamak boundary many times, whereas the red manifold seems to be bound to the chaotic region immediately surrounding the plasma magnetic surfaces with a few excursions

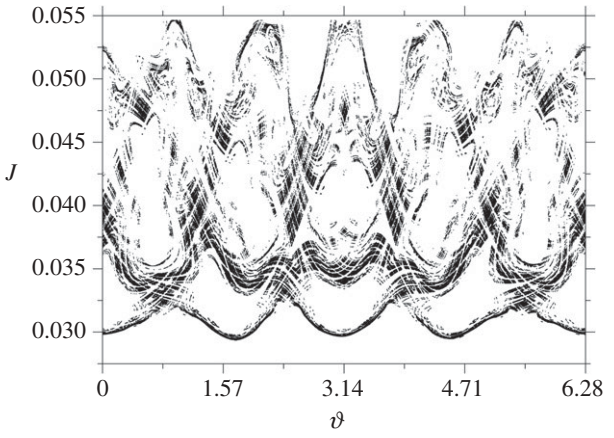

Figure 8. Chaotic saddle related to the invariant manifolds depicted in figure 7.

achieving the wall. This is ultimately a consequence of the non-uniformity of the limiter field, since the latter decays exponentially with the distance from the tokamak wall.

If we repeat the above-mentioned process for the backward iterates and retain only the grid points generating trajectories that do not hit the wall after n backward iterates, we have the stable manifold of the chaotic saddle (figure 7*b*). We have again a marked difference from the manifolds (coloured as light and deep blue) stemming from points with different radial locations with respect to the wall. The chaotic saddle can be also obtained from the sprinkler method by using a fraction of the iterates: $n' = \chi n$, with $0 < \chi < 1$ (see figure 8 for an example corresponding to the previously displayed manifolds). Points exactly on the chaotic saddle would remain there for all forward and backward iterations of the map. If a field line starts off but near the chaotic saddle, it will wander erratically along the homoclinic tangle, so as to approach arbitrarily close any unstable orbit embedded in the chaotic saddle.

The convoluted nature of the regions with same connection lengths, as revealed by figures 4 and 5, can be understood as a consequence of the dynamical properties of the chaotic saddle which underlies the chaotic layer near the tokamak wall and the corresponding manifold structure, more specifically the so-called *lambda lemma* [3]. We can make a 'coarse graining', by replacing the continuous colour scale used in figures 4 and 5 by a discrete scale with only two regions, namely one with connection lengths less than, say, 200 and the other one with more than 200. As a consequence there will be only two regions, to which we can assign black and white pixels. The boundary between the black and white region is a partitioning line.

We suppose now that this partitioning line crosses the stable or unstable manifold of the chaotic saddle. Thus, the boundary between the black and white regions is fractal. Since we may think of an arbitrarily large number of regions with values of connection length, the coloured regions in figures 4 and 5 form incursive fingers with the same fractal properties of the single partitioning line. A finite segment of the partitioning line is smoothly deformed before reaching the chaotic

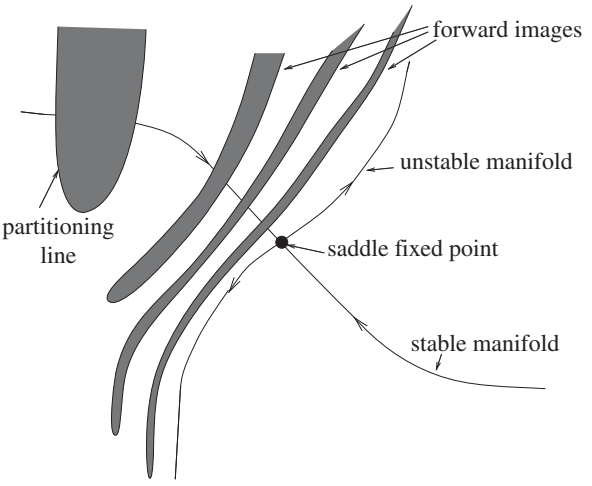

Figure 9. Schematic showing the formation of incursive fingers for regions with the same connection length.

saddle. Points lying exactly on its stable and unstable manifolds would remain attached to the chaotic saddle for any time. On the other hand, the segments of the partitioning line in between the manifolds become increasingly elongated and converge to the manifolds.

According to the scheme of figure 9, the forward images of the partitioning line approach the fixed point such that: (i) the intersection points between the stable manifold and the partitioning line converge exponentially fast according to the corresponding eigenvalue of the linearized map at the fixed point (with modulus less than unity), (ii) the lengths of the lobes increase exponentially in order to preserve areas, and (iii) the lobes tend to follow the unstable manifold [64]. The union of all images of the partitioning line is a wildly oscillating curve as it approaches the unstable fixed point, such that segments of the partitioning line accumulate on the filaments of the unstable manifold. If we consider the backward iterations the same conclusions hold, i.e. backward images of the partitioning line accumulate asymptotically on the filaments of the stable manifold.

6. Wada basins and magnetic footprints

In figures 4 and 5, the regions for which the connection lengths belong to a same interval are examples of the so-called *exit* or *escape basins*. These are defined as the sets of initial conditions which generate field lines escaping through a given exit [41,54,60]. This exit can be a material surface, such as a divertor plate, or simply a region we choose from any position along the tokamak region. As an example, we consider the tokamak wall as subdivided into three poloidal sections of equal length: $0 \leq \vartheta < 2\pi/3$, $2\pi/3 \leq \vartheta < 4\pi/3$ and $4\pi/3 \leq \vartheta < 2\pi$, corresponding to different exits for a chaotic field line.

To obtain the exit basins we used a fine grid of points chosen within the region depicted in figure 4*c*. The result, shown in figure 10*a*, is such that we colour the initial condition pixel in red, yellow or blue, depending on whether the field

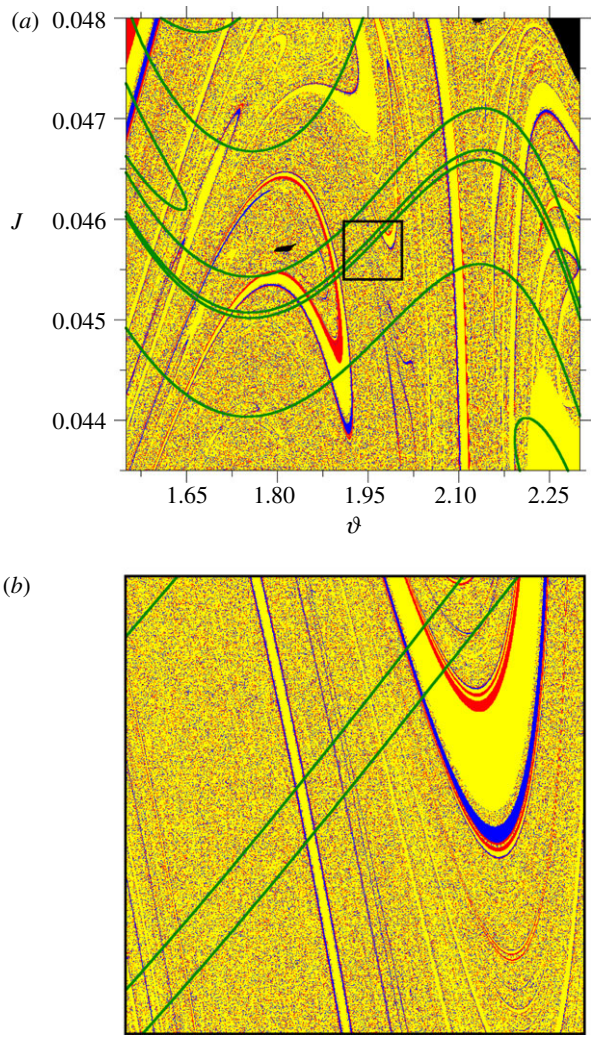

Figure 10. (*a*) Exit basins corresponding to the regions $0 \le \vartheta < 2\pi/3$ (red), $2\pi/3 \le \vartheta < 4\pi/3$ (yellow), and $4\pi/3 \le \vartheta < 2\pi$ (blue) of the tokamak wall, for points belonging to the region shown in figure 4*c*. We depict in green a part of the unstable manifold stemming from the point P_5 indicated in figure 7*a*. (*b*) Magnification of the box shown in (*a*). (Online version in colour.)

line hits the wall at one of the ϑ-intervals defined above. The regions with these colours are, thus, numerical approximations for the exit basins corresponding to these sections we choose at the wall. They are clearly intertwined in fine scales for some regions of the plasma. We illustrate this point by showing in figure 10*b* a magnification of a rectangle chosen in figure 10*a*. Inasmuch as the three exit basins are intermixed, the zoomed figure also shares the property, which repeats itself at *any* scale, no matter how fine. This property is actually stronger than that of fractal basin boundaries: the exit basins drawn in figure 10 have the so-called *Wada property* [7].

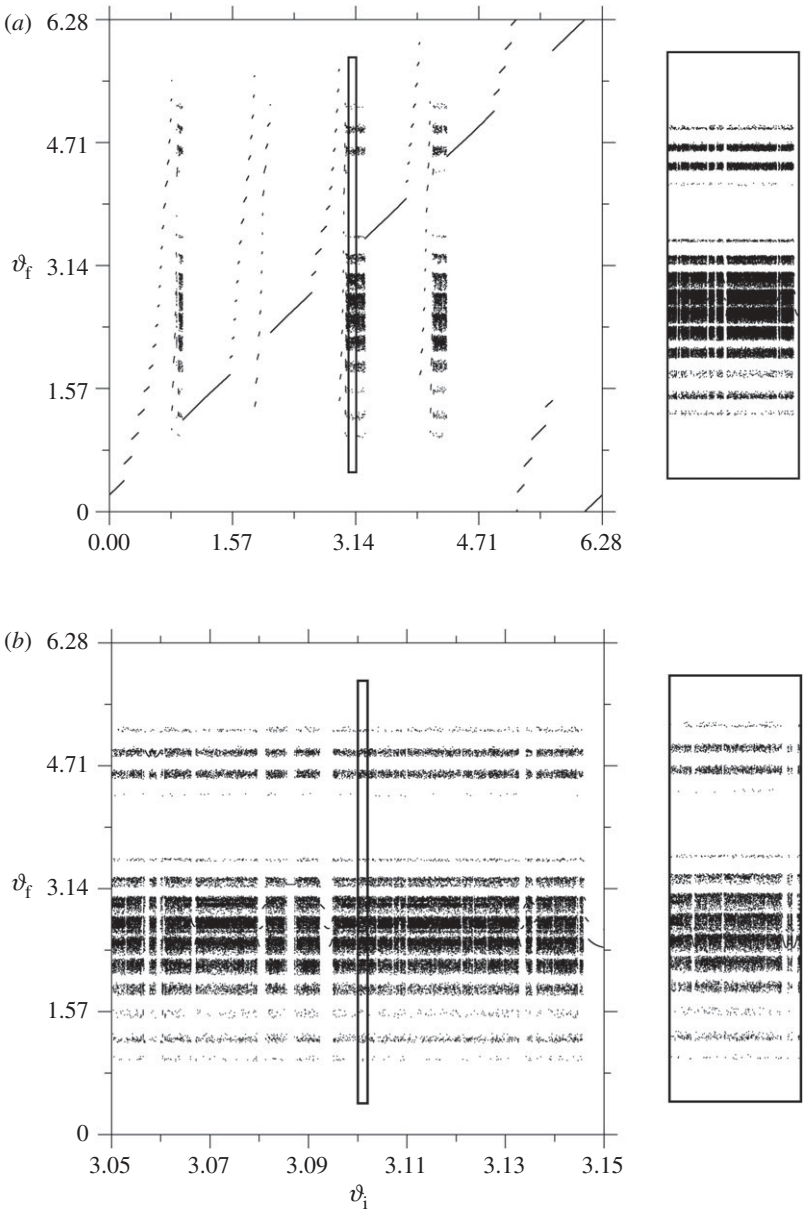

Figure 11. (*a*) Field line final poloidal angle at the tokamak wall versus initial poloidal angle; (*b*) a magnification of a rectangle picked up from (*a*).

In order to characterize this property we outline some basic definitions. Let us consider an exit basin $\mathcal{B}$, which may be any of those represented in figure 10*a*. A point p is a boundary point of the basin $\mathcal{B}$ if every open neighbourhood of p intersects the basin $\mathcal{B}$ and at least another basin. The basin boundary $\partial\mathcal{B}$ is the set of all boundary points of that basin. Moreover, the boundary point p is also a *Wada point* if every open neighbourhood of p intersects at least three different

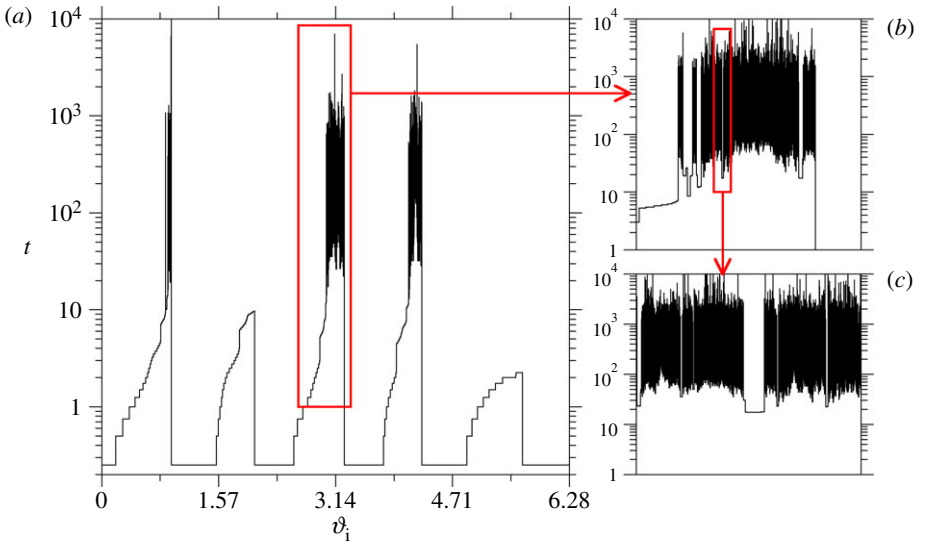

Figure 12. (*a*) Escape time versus initial poloidal angle for the case shown in figure 11. (*b*,*c*) Two magnifications of the fractal peak structure are shown. (Online version in colour.)

basins. A basin boundary $\partial\mathcal{B}$ has the Wada property if every boundary point of $\mathcal{B}$ is a Wada point [37–39]. A necessary (but not sufficient) condition that indicates that a basin boundary has the Wada property is that the unstable manifold of an unstable periodic point p must intersect every basin [40,65].

In our specific example this means that, after choosing an unstable fixed point p belonging to the boundary between exit basins, if it is a Wada point it is necessary that the unstable manifold which stems from this point intersects all other basins. From a rigorous point of view, at least one of the following complementary conditions has to be satisfied: (i) the stable manifold of the saddle point p must be dense in the boundary of the three regions, (ii) the periodic orbit p must be the only accessible orbit from the basin $\mathcal{B}$. Otherwise, every unstable manifold of other periodic orbits that are accessible from $\mathcal{B}$ must intersect all basins, and (iii) the periodic orbit p must generate a basin cell [63,66]. However, these conditions are extremely difficult to verify in practice.

Another fractal structure of interest for area-preserving maps related to field line diffusion through the tokamak wall is the magnetic footprints, having been intensively studied in the conceptual designs of divertor plates. A divertor has the function of channelling the field lines from undesired regions to a specific target with the goal of removing undesirable energetic particles from the plasma edge [24–28,30]. The divertor surface is thus hit by these particles such that, if the field line traces are too narrowly concentrated, this could lead to overheating and even damage of portions of the collector plate.

A slightly different version of this situation appears if we choose a given boundary (like those used for defining exit basins) and consider the magnetic footprints as traces of field lines with some specified property. Let us consider a field line originating from a point belonging to the tokamak wall at some 'initial' angle ϑ_i, which occurs after a number of map iterations, which is

different for each point in general. We then follow this field line until it reaches back to the tokamak wall, and save the corresponding 'final' angle ϑ_f. In figure 11*a* we plot the initial angle versus the final angle for a number of initial conditions originated from the wall, revealing a striped pattern with a self-similar structure along the angular direction, as suggested by the magnification shown in figure 11*b*. A further example of this self-similarity is the angular dependence of the number of the map iterations it takes for a field line to return to the wall after being commenced there (figure 12*a*, with magnifications in figure 12*b*,*c*). We may think of t as being an escape time, and its dependence on the angle is likely to have the same characteristics of the fractality inherent to the chaotic saddle.

7. Conclusions

Fractal structures are ubiquitous in nonlinear dynamics, particularly in chaotic invariant sets like strange attractors. In area-preserving maps, one outstanding example of fractal structure is the chaotic saddle, which is a non-attractive invariant set possessing an infinite number of unstable periodic orbits. In area-preserving maps with physical interest, we are naturally inclined to seek for observable manifestations of such chaotic saddles. It turns out that, in the plasma physics context, we can investigate such fractal structures in the chaotic region of the field line Lagrangian flow in a tokamak with ergodic limiters. In this specific context, the formation of the chaotic region is essential to the ultimate goal of such devices, namely to create a 'cold' boundary layer of field lines so as to distribute uniformly heat and particle loadings on the tokamak wall. However, the experimental evidences do not quite agree with these expectations, for the deposition patterns, while still requiring a chaotic region to be obtained, are not uniform and rather present a self-similar structure. This fact is a consequence of the fractal structures like the chaotic saddle underlying the chaotic region of the field line map.

We considered in this work some of these structures. First, connection lengths measure the 'time' (in number of tokamak turns) it takes for a field line, originated in the chaotic region, to hit the wall. The fractal nature of these regions is a direct consequence of the behaviour of a partitioning line which crosses an invariant manifold of an unstable orbit belonging to the chaotic saddle. Second, we have shown the formation of magnetic footprints, which are traces of field lines hitting the tokamak wall, and which exhibit a self-similar dependence on the angular position there. Third, we have verified the Wada property when three exit basins are considered. An exit basin is the set of initial conditions originating field lines hitting the wall at some specified angular position interval.

Although we have considered the presence and effect of fractal structures in the dynamics of magnetic field lines, we believe that our findings will shed some light on the (more difficult) problem of how plasma particles would behave in chaotic magnetic fields. Moreover, the latter problem opens a new horizon for it allows us to relate the statistical properties of diffusion with the field line dynamics. One example is the relation between the connection lengths and the recurrence times [67–69]. The information we get from the magnetic field line description can be thus used to investigate charged particle behaviour,

particularly in situations involving electromagnetic turbulence, which is an intrinsically mesoscopic phenomenon in plasmas. For example, transport barriers are regions in the tokamak plasma where the turbulent transport is significantly reduced. Such transport barriers are present when there are dimerized magnetic islands owing to non-monotonic plasma current profiles and reversed magnetic shear [60,70,71].

This work was made possible with partial financial help from FAPESP, CNPq, CAPES and FINEP/CNEN (Brazilian Fusion Network). M.A.F.S. acknowledges financial support from the Spanish Ministry of Education and Science under project no. FIS2006-08525 and from the Spanish Ministry of Science and Innovation under project no. FIS2009-09898, and the hospitality of Beijing Jiaotong University under the Key Invitation Program for Top-Level Experts of the State Administration of Foreign Experts Affairs of China.

References

1 Mandelbrot, B. B. 2004 *Fractals and chaos: the Mandelbrot set and beyond*. New York, NY: Springer.
2 Ott, E. 1993 *Chaos in dynamical systems*. New York, NY: Cambridge University Press.
3 Alligood, K. T., Sauer, T. D. & Yorke, J. A. 1996 *Chaos: an introduction to dynamical systems*. New York, NY: Springer.
4 McDonald, S. W., Grebogi, C., Ott, E. & Yorke, J. A. 1985 Fractal basin boundaries. *Physica D* **17**, 125–153. (doi:10.1016/0167-2789(85)90001-6)
5 Smale, S. 1967 Differentiable dynamical systems. *Bull. Am. Math. Soc.* **73**, 747–817. (doi:10.1090/S0002-9904-1967-11798-1)
6 Devaney, R. L. 2003 *An introduction to chaotic dynamical systems*, 2nd edn. Boulder, CO: Westview Press.
7 Aguirre, J., Viana, R. L. & Sanjuán, M. A. F. 2009 Fractal structures in nonlinear dynamics. *Rev. Mod. Phys.* **81**, 333–386. (doi:10.1103/RevModPhys.81.333)
8 Wesson, J. 1987 *Tokamaks*. Oxford, UK: Oxford University Press.
9 Hazeltine, R. D. & Meiss, J. D. 1991 *Plasma confinement*. Reading, MA: Addison-Wesley.
10 Kadomtsev, B. B. 1992 *Tokamak plasma: a complex physical system*. Bristol, UK: Institute of Physics.
11 Itoh, K., Itoh, S.-I. & Fukuyama, A. 1999 *Transport and structural formation in plasmas*. Bristol, UK: Institute of Physics.
12 Thyagaraja, A., Knight, P. J. & Loureiro, N. 2004 Mesoscale plasma dynamics, transport barriers and zonal flows: simulations and paradigms. *Eur. J. Mech. B* **23**, 475–490. (doi:10.1016/j.euromechflu.2003.10.009)
13 Lichtenberg, A. J. & Lieberman, M. A. 1992 *Regular and chaotic dynamics*, 2nd edn. New York, NY: Springer.
14 Spatschek, K. H. 2008 Aspects of stochastic transport in laboratory and astrophysical plasmas. *Plasma Phys. Contr. Fusion* **50**, 124027. (doi:10.1088/0741-3335/50/12/124027)
15 Balescu, R., Vlad, M. & Spineanu, F. 1998 Tokamap: a Hamiltonian twist map for magnetic field lines in a toroidal geometry. *Phys. Rev. E* **58**, 951–964. (doi:10.1103/PhysRevE.58.951)
16 Caldas, I. L., Viana, R. L., Araujo, M. S. T., Vannucci, A., da Silva, E. C., Ullmann, K. & Heller, M. V. A. P. 2002 Control of chaotic magnetic fields in tokamaks. *Braz. J. Phys.* **32**, 980–1004. (doi:10.1590/S0103-97332002000500023)
17 Abdullaev, S. S. 2006 *Construction of mappings for Hamiltonian systems and their applications*. New York, NY: Springer.
18 Martin, T. J. & Taylor, J. B. 1984 Ergodic behavior in a magnetic limiter. *Plasma Phys. Contr. Fusion* **26**, 321. (doi:10.1088/0741-3335/26/1B/005)
19 Ullmann, K. & Caldas, I. L. 2000 A symplectic mapping for the ergodic magnetic limiter and its dynamical analysis. *Chaos, Solitons Fractals* **11**, 2129–2140. (doi:10.1016/S0960-0779(99)00138-1)
20 da Silva, E. C., Caldas, I. L. & Viana, R. L. 2001 Field line diffusion and loss in a tokamak with an ergodic magnetic limiter. *Phys. Plasmas* **8**, 2855–2865. (doi:10.1063/1.1371769)

21 da Silva, E. C., Caldas, I. L. & Viana, R. L. 2001 The structure of chaotic magnetic field lines in a tokamak with external nonsymmetric magnetic perturbations. *IEEE Trans. Plasma Sci.* **29**, 617–631. (doi:10.1109/27.940957).

22 Karger, F. & Lackner, K. 1977 Resonant helical divertor. *Phys. Lett. A* **61**, 385–387. (doi:10.1016/0375-9601(77)90341-3)

23 Engelhardt, W. & Feneberg, W. 1978 Influence of an ergodic magnetic limiter on the impurity content in a tokamak. *J. Nucl. Mater.* **76/77**, 518–520. (doi:10.1016/0022-3115(78)90198-8)

24 Punjabi, A., Verma, A. & Boozer, A. 1992 Stochastic broadening of the separatrix of a tokamak divertor. *Phys. Rev. Lett.* **69**, 3322–3325. (doi:10.1103/PhysRevLett.69.3322)

25 Punjabi, A., Ali, H. & Boozer, A. 1997 Symmetric simple map for a single-null divertor tokamak. *Phys. Plasmas* **4**, 337–346. (doi:10.1063/1.872094)

26 Abdullaev, S. S., Finken, K. H., Kaleck, A. & Spatschek, K. H. 1998 Twist mapping for the dynamics of magnetic field lines in a tokamak ergodic divertor. *Phys. Plasmas* **5**, 196–210. (doi:10.1063/1.872689)

27 Abdullaev, S. S., Finken, K. H. & Spatschek, K. H. 1999 Asymptotical and mapping methods in study of ergodic divertor magnetic field in a toroidal system. *Phys. Plasmas* **6**, 153–174. (doi:10.1063/1.873270)

28 Ali, H., Punjabi, A., Boozer, A. & Evans, T. E. 2004 The low MN map for single-null divertor tokamaks. *Phys. Plasmas* **11**, 1908–1919. (doi:10.1063/1.1691455)

29 Evans, T. E., Roeder, R. K. W., Carter, J. A. & Rapoport, B. I. 2004 Homoclinic tangles, bifurcations and edge stochasticity in diverted tokamaks. *Contrib. Plasma Phys.* **44**, 235–240. (doi:10.1002/ctpp.200410034)

30 Kroetz, T., Roberto, M., Caldas, I. L., Viana, R. L., Morrison, P. J. & Abbamonte, P. 2010 Integrable maps with topological applications to divertor configurations. *Nucl. Fusion* **50**, 034003. (doi:10.1088/0029-5515/50/3/034003)

31 Evans, T. E., Moyer, R. A. & Monat, P. 2002 Modelling of stochastic magnetic flux loss from the edge of a poloidally diverted tokamak. *Phys. Plasmas* **9**, 4957–4967. (doi:10.1063/1.1521125)

32 Wingen, A., Jakubowski, M., Spatschek, K. H., Abdullaev, S. S., Finken, K. H. & Lehnen, M. 2007 Traces of stable and unstable manifolds in heat flux patterns. *Phys. Plasmas* **14**, 042502. (doi:10.1063/1.2715548)

33 Abdullaev, S. S., Jakubowski, M., Lehnen, M., Schmitz, O. & Unterberg, B. 2008 On description of magnetic stochasticity in poloidal divertor tokamaks. *Phys. Plasmas* **15**, 042508. (doi:10.1063/1.2907163)

34 Borgogno, D., Grasso, D., Pegoraro, F. & Schep, T. J. 2008 Stable and unstable invariant manifolds in a partially chaotic magnetic configuration generated by nonlinear reconnection. *Phys. Plasmas* **15**, 102308. (doi:10.1063/1.2999539)

35 da Silva, E. C., Caldas, I. L., Viana, R. L. & Sanjuán, M. A. F. 2002 Escape patterns, magnetic footprints, and homoclinic tangles due to ergodic magnetic limiters. *Phys. Plasmas* **9**, 4917–4928. (doi:10.1063/1.1518681)

36 Wingen, A., Spatschek, K. H. & Abdullaev, S. S. 2005 Stochastic transport of magnetic field lines in the symmetric tokamap. *Contrib. Plasma Phys.* **45**, 500–513. (doi:10.1002/ctpp.200510056)

37 Kennedy, J. & Yorke, J. A. 1991 Basins of Wada. *Physica D* **51**, 213–225. (doi:10.1016/0167-2789(91)90234-Z)

38 Nusse, H. E. & Yorke, J. A. 1996 Basins of attraction. *Science* **271**, 1376–1380. (doi:10.1126/science.271.5254.1376)

39 Nusse, H. E. & Yorke, J. A. 1996 Wada basin boundaries and basin cells. *Physica D* **90**, 242–261. (doi:10.1016/0167-2789(95)00249-9)

40 Aguirre, J., Vallejo, J. C. & Sanjuán, M. A. F. 2001 Wada basins and chaotic invariant sets in the Hénon–Heiles system. *Phys. Rev. E* **64**, 066208. (doi:10.1103/PhysRevE.64.066208)

41 Abdullaev, S. S., Eich, T. & Finken, K. H. 2001 Fractal structure of the magnetic field in the laminar zone of the dynamic ergodic divertor of the torus experiment for technology-oriented research (TEXTOR-94). *Phys. Plasmas* **8**, 2739–2749. (doi:10.1063/1.1371954)

42 Schmidt, G. 1979 *Physics of high-temperature plasmas*, 2nd edn. New York, NY: Academic Press.

43 D'haeseleer, W. D., Hitchon, W. N. G., Callen, J. D. & Shohet, J. L. 1991 *Flux coordinates and magnetic field structure*. Berlin, Germany: Springer.
44 Kucinski, M. Y. & Caldas, I. L. 1987 Toroidal helical fields. *Z. Naturforsch. A* **42**, 1124.
45 Kucinski, M. Y., Caldas, I. L., Monteiro, L. H. A. & Okano, V. 1990 Toroidal plasma equilibrium with arbitrary current distribution. *J. Plasma Phys.* **14**, 303–311. (doi:10.1017/S0022377800015191)
46 Morrison, P. J. 2000 Magnetic field lines, Hamiltonian dynamics, and nontwist systems. *Phys. Plasmas* **7**, 2279–2289. (doi:10.1063/1.874062)
47 Hinton, F. L. & Hazeltine, R. D. 1974 Kinetic theory of plasma scrape-off in a divertor tokamak. *Phys. Fluids* **17**, 2236–2240. (doi:10.1063/1.1694697)
48 McCool, S. C. *et al.* 1989 Electron thermal confinement studies with applied resonant fields on TEXT. *Nucl. Fusion* **29**, 547–562.
49 Ghendrih, P., Grosman, A. & Capes, H. 1996 Theoretical and experimental investigations of stochastic boundaries in tokamaks. *Plasma Phys. Contr. Fusion* **38**, 1653. (doi:10.1088/0741-3335/38/10/002)
50 Pires, C. J. A., Saettone, E. A. O., Kucinski, M. Y., Vannucci, A. & Viana, R. L. 2005 Magnetic field structure in the TCABR tokamak due to ergodic limiters with a non-uniform current distribution: theoretical and experimental results. *Plasma Phys. Contr. Fusion* **47**, 1609. (doi:10.1088/0741-3335/47/10/003)
51 Viana, R. L. & Vasconcelos, D. B. 1997 Field-line stochasticity in a tokamak with an ergodic magnetic limiter. *Dynam. Stability Syst.* **12**, 75–88.
52 Boozer, A. & Rechester, A. B. 1978 Effect of magnetic perturbations on divertor scrape-off width. *Phys. Fluids* **21**, 682–680. (doi:10.1063/1.862277)
53 Meiss, J. D. 1992 Symplectic maps, variational principles, and transport. *Rev. Mod. Phys.* **64**, 795–848. (doi:10.1103/RevModPhys.64.795)
54 Portela, J. S. E., Caldas, I. L. & Viana, R. L. 2008 Tokamak magnetic field line structure described by simple maps. *Eur. Phys. J.: Special Topics* **165**, 195–210. (doi:10.1140/epjst/e2008-00863-y)
55 Bleher, S., Grebogi, C., Ott, E. & Brown, R. 1988 Fractal boundaries for exit in Hamiltonian dynamics. *Phys. Rev. A* **38**, 930–938. (doi:10.1103/PhysRevA.38.930)
56 Schneider, J., Tel, T. & Neufeld, Z. 2002 Dynamics of 'leaking' Hamiltonian systems. *Phys. Rev. E* **66**, 066218. (doi:10.1103/PhysRevE.66.066218)
57 Aguirre, J. & Sanjuán, M. A. F. 2003 Limit of small exits in open Hamiltonian systems. *Phys. Rev. E* **67**, 056201. (doi:10.1103/PhysRevE.67.056201)
58 Sanjuán, M. A. F., Horita, T. & Aihara, H. 2003 Opening a closed Hamiltonian map. *Chaos* **13**, 17–24. (doi:10.1063/1.1528750)
59 Abdullaev, S. S., Finken, K. H., Jakubowski, M. W., Kasilov, S., Kobayashi, V. M., Reiser, D., Reiter, D., Runov, A. M. & Wolf, R. 2003 Overview of magnetic structure induced by the TEXTOR-DED and the related transport. *Nucl. Fusion* **43**, 299–313. (doi:10.1088/0029-5515/43/5/302)
60 Kroetz, T., Roberto, M., da Silva, E. C., Caldas, I. L. & Viana, R. L. 2008 Escape patterns of chaotic magnetic field lines in a tokamak with reversed magnetic shear and an ergodic limiter. *Phys. Plasmas* **15**, 092310. (doi:10.1063/1.2988335)
61 Schmitz, O. *et al.* 2008 Aspects of three dimensional transport for ELM control experiments in ITER-similar shape plasmas at low collisionality in DIII-D. *Plasma Phys. Contr. Fusion* **50**, 124029. (doi:10.1088/0741-3335/50/12/124029)
62 Péntek, A., Toroczkai, Z., Tél, T., Grebogi, C. & Yorke, J. A. 1995 Fractal boundaries in open hydrodynamical flows: signatures of chaotic saddles. *Phys. Rev. E* **51**, 4076–4088. (doi:10.1103/PhysRevE.51.4076)
63 Poon, L., Campos, J., Ott, E. & Grebogi, C. 1996 Wada basin boundaries in chaotic scattering. *Int. J. Bifurc. Chaos* **6**, 251–265. (doi:10.1142/S0218127496000035)
64 MacKay, R. S., Meiss, J. D. & Percival, I. C. 1987 Resonances in area-preserving maps. *Physica D* **27**, 1–20. (doi:10.1016/0167-2789(87)90002-9)
65 Aguirre, J. & Sanjuán, M. A. F. 2002 Unpredictable behavior in the Duffing oscillator: Wada basins. *Physica D* **171**, 41–51. (doi:10.1016/S0167-2789(02)00565-1)

66 Toroczkai, Z., Károlyi, G., Péntek, A., Tél, T., Grebogi, C. & Yorke, J. A. 1997 Wada dye boundaries in open hydrodynamical flows. *Physica A* **239**, 235–243. (doi:10.1016/S0378-4371(96)00482-7)

67 Baptista, M. S., Caldas, I. L., Heller, M. V. A. P., Ferreira, A. A., Bengtson, R. & Stockel, J. 2001 Recurrence in plasma edge turbulence. *Phys. Plasmas* **8**, 4455–4462. (doi:10.1063/1.1401117)

68 Altmann, E. G., da Silva, E. C. & Caldas, I. L. 2004 Recurrence time statistics for finite size intervals. *Chaos* **14**, 975–981. (doi:10.1063/1.1795491)

69 Zaslavsky, G. M. 2005 *Hamiltonian chaos and fractional dynamics*. Oxford, UK: Oxford University Press.

70 Marcus, F. A., Kroetz, T., Roberto, M., Caldas, I. L., da Silva, E. C., Viana, R. L. & Guimarães-Filho, Z. O. 2008 Chaotic transport in reversed-shear tokamaks. *Nucl. Fusion* **48**, 024018. (doi:10.1088/0029-5515/48/2/024018)

71 Kroetz, T., Marcus, F. A., Roberto, M., Caldas, I. L. & Viana, R. L. 2009 Transport control in fusion plasmas by changing electric and magnetic field spatial profiles. *Comput. Phys. Commun.* **180**, 642–650. (doi:10.1016/j.cpc.2008.12.025)